Nano Res. 2011, 4(12): 1233–1241
DOI 10.1007/s12274-011-0174-1
Research Article

ISSN 1998-0124
CN 11-5974/O4

One-Step Synthesis of Magnetically Recyclable Au/Co/Fe Triple-Layered Core–Shell Nanoparticles as Highly Efficient Catalysts for the Hydrolytic Dehydrogenation of Ammonia Borane

Kengo Aranishi[1,2], Hai-Long Jiang[1], Tomoki Akita[1,4], Masatake Haruta[3,4], and Qiang Xu[1,2,4] (✉)

[1] National Institute of Advanced Industrial Science and Technology (AIST), Ikeda, Osaka 563-8577, Japan
[2] Graduate School of Engineering, Kobe University, Nada Ku, Kobe, Hyogo 657-8501, Japan
[3] Graduate School of Urban Environmental Sciences, Tokyo Metropolitan University, Minami-Osawa, Hachioji, Tokyo 192-0397, Japan
[4] Core Research for Evolutional Science and Technology (CREST), Japan Science and Technology Agency (JST), Kawaguchi, Saitama 332-0012, Japan

Received: 23 March 2011 / Revised: 13 August 2011 / Accepted: 1 September 2011

ABSTRACT

Magnetically recyclable Au/Co/Fe core–shell nanoparticles (NPs) have been successfully synthesized via a one-step *in situ* procedure. Transmission electron microscope (TEM), energy dispersive X-ray spectroscopic (EDS), and electron energy-loss spectroscopic (EELS) measurements revealed that the trimetallic Au/Co/Fe NPs have a triple-layered core–shell structure composed of a Au core, a Co-rich inter-layer, and a Fe-rich shell. The Au/Co/Fe core–shell NPs exhibit much higher catalytic activities for hydrolytic dehydrogenation of ammonia borane (NH_3BH_3, AB) than the monometallic (Au, Co, Fe) or bimetallic (AuCo, AuFe, CoFe) counterparts.

KEYWORDS

Triple-layered, core–shell nanoparticles, heterogeneous catalysis, ammonia borane, hydrogen generation

1. Introduction

Heterometallic nanoparticles (NPs) have attracted growing attention in recent years owing to their unique and novel properties, which are often very different from those of the monometallic counterparts [1–16]. The incorporation of magnetic elements in NPs will expand their applications to biomedical operations, information storage, and heterogeneous catalysis [15, 16]. Therefore, studies of the synthesis and applications of magnetic alloy NPs are of great interest in terms of seeking synergistic structural and electronic effects combined with the intrinsic properties of the magnetic element. There have been a considerable number of investigations of core–shell structured bimetallic magnetic NPs [16–18], whereas magnetic core–shell NPs with a triple-layered structure are, to the best of our knowledge, rare [18–20]. Triple-layered trimetallic NPs might have superior physicochemical (especially catalytic) performances to their monometallic/bimetallic counterparts because their electronic structures are more tunable [6, 21]. Toshima and coworkers have fabricated ~3 nm Au/Pt/Rh trimetallic NPs by simple mixing of bimetallic Au/Pt NPs and monometallic Rh NPs [18]. Sun and coworkers have obtained ~6 nm Pd/Au/FePt core–shell NPs via a multi-step synthetic approach [19]. Yamauchi and coworkers have reported the one-step synthesis

Address correspondence to q.xu@aist.go.jp

of multifunctional Au/Pd/Pt core–shell NPs with an average particle diameter of 35 nm [20]. Developing a facile one-step route to construct triple-layered non-noble metal-containing core–shell NPs with small particle sizes and with high catalytic activities still remains a considerable challenge, however.

Currently, a great deal of work has been devoted to the development of effective hydrogen storage materials for hydrogen fuel cells and hydrogen energy systems. Ammonia borane (NH_3BH_3, AB) has a hydrogen capacity as high as 19.6 wt.%, which exceeds that of gasoline, and is accordingly an attractive candidate for chemical hydrogen-storage [22–36]. Hydrogen can be generated by thermal decomposition of AB [23–26], but catalytic hydrolysis provides an alternative route for hydrogen generation under milder conditions [12, 27–36]. One of the major requirements for practical application of the catalytic decomposition is to develop efficient, economical, and easily recyclable catalysts.

Herein, we report a facile one-step seeding-growth method for preparing magnetically recyclable Au/Co/Fe triple-layered core–shell NPs around 10 nm in diameter under ambient conditions. Compared with their mono-metallic and bimetallic counterparts, the Au/Co/Fe triple-layered core–shell NPs exhibit remarkably enhanced catalytic activity for the hydrolytic dehydrogenation of aqueous AB.

2. Experimental details

2.1 Chemicals

Ammonia borane (NH_3BH_3, AB, JSC Aviabor, 97%), iron (Ⅲ) chloride hexahydrate ($FeCl_3{\cdot}6H_2O$, Sigma–Aldrich Japan, 99.0%), cobalt (Ⅱ) chloride hexahydrate ($CoCl_2{\cdot}6H_2O$, Wako Pure Chemical Industries, Ltd., > 99%), hydrogen tetrachloroaurate (Ⅲ) tetrahydrate ($HAuCl_4{\cdot}4H_2O$, Wako Pure Chemical Industries, Ltd., > 99%), polyvinylpyrrolidone K 30 (PVP, $(C_6H_9NO)_n$, *M*w: av. 40,000, Tokyo Chemical Industry Co., Ltd.), platinum (Ⅳ) dioxide ($PtO_2{\cdot}nH_2O$, Mitsuwa Chemicals Co., Ltd., Pt > 78.8%), and ethanol (CH_3CH_2OH, Kishida Chemical Co., Ltd., > 99.8%) were used as received. Deionized H_2O with a specific resistance of 17.5 M·Ω cm was obtained by reversed osmosis followed by ion-exchange and filtration (RFD250NB, Toyo Roshi Kaisha, Ltd., Japan).

2.2 Physical characterization

Ultraviolet-visible (UV–Vis) absorption spectra were recorded on a Shimadzu UV-2550 spectrophotometer in the wavelength range 300–800 nm and corrected using aqueous PVP (1 wt.%) solution as background absorption. Transmission electron microscope (TEM, JEOL JEM-3000F), high-angle annular dark-field scanning TEM (HAADF-STEM), energy-dispersive X-ray spectroscopy (EDS), and electron energy-loss spectroscopy (EELS) were used for the determination of detailed microstructure and composition. The TEM (HAADF-STEM, EDS, EELS) samples were prepared by depositing one or two droplets of the NPs suspended in the reaction solution onto amorphous carbon-coated copper grids, which were then dried in an argon atmosphere. Powder X-ray diffraction (XRD) was performed on a Rigaku RINT-2000 X-ray diffractometer with Cu *Kα* radiation. A glass substrate holding the powder sample was covered by an adhesive tape on the surface to prevent the sample from exposure to air during the measurements. Mass analysis of the generated gases was performed using a Balzers Prisma QMS 200 mass spectrometer.

2.3 Synthesis of Au/Co/Fe triple-layered core–shell NPs

In a typical experiment, 5.0 mg of $HAuCl_4{\cdot}4H_2O$ (0.012 mmol), 2.9 mg of $CoCl_2{\cdot}6H_2O$ (0.012 mmol), and 48.1 mg of $FeCl_3{\cdot}6H_2O$ (0.176 mmol) were dissolved along with PVP (100 mg) in 10.0 mL of water (giving a molar ratio of Au∶Co∶Fe = 6∶6∶88). The solution of metal salt precursors was shaken (220 r/min) at room temperature for 2 min and then 55.0 mg of NH_3BH_3 was added while shaking. Magnetic stirring was not employed because of the aggregation of the prepared magnetic particles caused by the strong magnet. The synthetic progress was monitored by UV–Vis spectroscopy. The as-prepared samples were used for XRD and TEM measurements.

2.4 Synthesis of bimetallic NPs

A similar procedure to that described above for the preparation of triple-layered NPs was employed. For

Au/Fe NPs, 5.0 mg of $HAuCl_4 \cdot 4H_2O$ (0.012 mmol) and 48.1 mg of $FeCl_3 \cdot 6H_2O$ (0.176 mmol) were used. For the synthesis of Au/Co NPs, 5.0 mg of $HAuCl_4 \cdot 4H_2O$ (0.012 mmol) and 2.9 mg of $CoCl_2 \cdot 6H_2O$ (0.012 mmol) were used. For the synthesis of Co/Fe NPs, 2.9 mg of $CoCl_2 \cdot 6H_2O$ (0.012 mmol) and 48.1 mg of $FeCl_3 \cdot 6H_2O$ (0.176 mmol) were used.

2.5 Synthesis of monometallic Au, Co, and Fe NPs

5.0 mg of $HAuCl_4$ (0.012 mmol), 2.9 mg of $CoCl_2$ (0.012 mmol), and 48.1 mg of $FeCl_3$ (0.176 mmol) were used for the syntheses of Au NPs, Co NPs, and Fe NPs, respectively. The procedure was similar to those for the triple-layered NPs and the bimetallic NPs.

2.6 Catalytic hydrolysis of AB

The *in situ* synthesized mono- and heterometallic NPs were directly used for catalytic hydrolysis of AB. Typically, 55.0 mg of AB was fed into a two-necked round-bottom flask, with one neck connected to a gas burette, and the other connected to a pressure-equalizing funnel to introduce the metal salt precursor(s) in 1 wt.% aqueous PVP solution (10.0 mL). The reaction started when the starting material in aqueous PVP solution was added to AB with vigorous shaking. The evolution of H_2, which was identified by mass spectrometry, was monitored using a gas burette. The reactions were carried out at room temperature under ambient atmosphere (Eq. (1)).

$$NH_3BH_3 + 2H_2O \longrightarrow NH_4^+ + BO_2^- + 3H_2 \quad (1)$$

2.7 Durability tests of the *in situ* synthesized Au/Co/Fe triple-layered core–shell NPs

The prepared Au/Co/Fe triple-layered core–shell NPs were isolated from the reaction solution by a magnet when hydrogen generation was complete. A new catalytic run was started by adding an additional equivalent amount of aqueous AB solution (55.0 mg AB in 10.0 mL of water) and the evolution of gas was monitored as described above.

2.8 Heat treatment of the as-synthesized Au/Co/Fe triple-layered core–shell NPs

The synthesized Au/Co/Fe triple-layered core–shell NPs were washed twice by water and once with ethanol. The sample was dried in a vacuum oven at room temperature and was then transferred into a furnace where a continuous He gas flow was introduced at the rate of 90 mL/min. The furnace temperature was elevated to 873 K and maintained at this value for 5 h. XRD patterns of the material before and after heat treatment were recorded.

3. Results and discussion

The one-step synthetic method for the Au/Co/Fe triple-layered core–shell NPs involved exposing a mixture of Au^{3+}, Co^{2+}, and Fe^{3+} precursors to the reducing agent at the same time. The basic concept is to take advantage of the difference in the reduction potentials of the three soluble metal cations ($E^o_{Fe(III)/Fe(II)}$ = +0.77 V vs. the standard hydrogen electrode (SHE); $E^o_{Fe(II)/Fe}$ = –0.44 V vs. SHE; $E^o_{Co(II)/Co}$ = –0.28 V vs, SHE; $E^o_{Au(III)/Au}$ = +0.93 V vs. SHE), which are a measure of their tendency to undergo reduction. Alcohols and ascorbic acid have been used as the reducing agents for the one-step synthesis of core–shell NPs of three noble metals [18, 20], but these are not applicable to non-noble metal-containing trimetallic core–shell NPs. In this work, AB was employed as the reducing agent, since the core Au NPs can be formed within a few seconds and then serve as *in situ* seeds for the successive catalytic reduction leading to the growth of the outer layers. Without Au cores, Fe and Co NPs cannot be formed because of their lower standard reduction potentials and the weak reduction capability of AB (even though Fe^{3+} can be reduced to Fe^{2+}). Formation of the Au cores leads to the slow release of H_2, inducing the reduction of Co^{2+} and growth of a Co-rich layer. Finally, the presence of the Au/Co core–shell NPs results in the rapid generation of H_2, which reduces Fe^{2+} to form a Fe-rich outer shell. The Au/Co/Fe triple-layered core–shell NPs are thus formed through successive reduction processes. On the basis of the difference in the reduction potentials of the three metal ions, a moderate reducing agent such as AB is essential.

The synthesis process can be monitored by the evolution of the solution color (Fig. 1). Under typical experimental conditions, once the aqueous solution

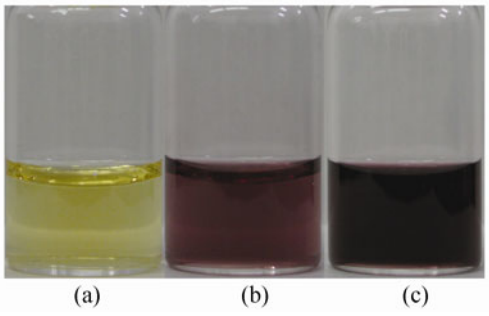

Figure 1 Color evolution during the formation of Au/Co/Fe core–shell NPs via a one-step seeding-growth method at room temperature. (a) Before, and (b) 10 s and (c) 1 min after adding AB to the aqueous PVP solution containing Au^{3+}, Co^{2+}, and Fe^{3+} precursors

of $HAuCl_4$, $CoCl_2$, and $FeCl_3$ with a molar ratio of 6:6:88 in the presence of PVP (1 wt.%) as the stabilizing agent was mixed with the solid AB, the color of the mixture immediately changed from its original light-yellow color (Fig. 1(a)) to wine-red (Fig. 1(b)) in a few seconds, indicating that Au^{3+} cations are preferentially reduced to Au^0 NPs prior to reduction of Co^{2+} and Fe^{3+} cations. Then the Au NPs serve as seeds for successive growth of Co and Fe shells during the H_2 generation. Accordingly, the solution color darkened to black within 1 min (Fig. 1(c)). Based on this color evolution and their intrinsic difference in reduction potentials, we can reasonably assume that the resulting particles have a core–shell architecture.

This assumption has been confirmed by monitoring the UV–Vis spectra (Fig. 2). No peaks can be observed before the addition of AB (Fig. 2(a)), whereas 10 s after introducing AB a distinct peak appears at 540 nm (Fig. 2(b)). This peak arises from the surface plasmon absorption of Au NPs. Then this characteristic peak broadens quickly and disappears completely in 2 min (Fig. 2(c)) due to the broad and strong absorption of the Co and Fe layers in the same spectral region with Au cores. The consistent evolution of color and UV–Vis spectra present strong evidence for the formation of a Au/Co/Fe core–shell architecture.

TEM images of the Au/Co/Fe triple-layered core–shell NPs with different magnification are shown in Fig. 3. The NPs are roughly spherical in shape and ~10 nm in size. The observed contrast in the NP structure indicates the formation of core, inter-layer, and outer

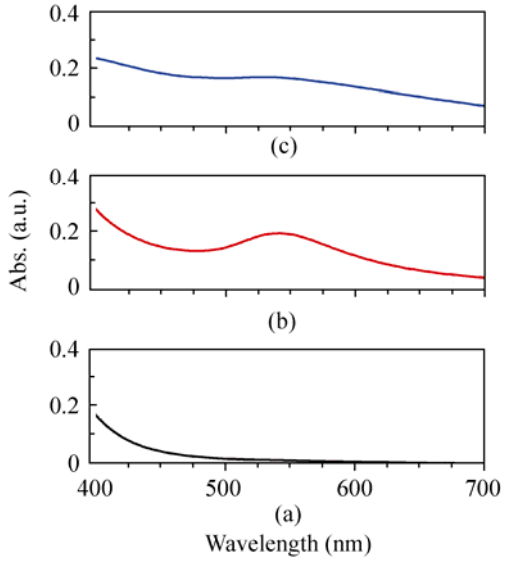

Figure 2 UV–Vis spectra during the synthesis of Au/Co/Fe core–shell NPs at reaction times of (a) 0 s, (b) 10 s, and (c) 120 s

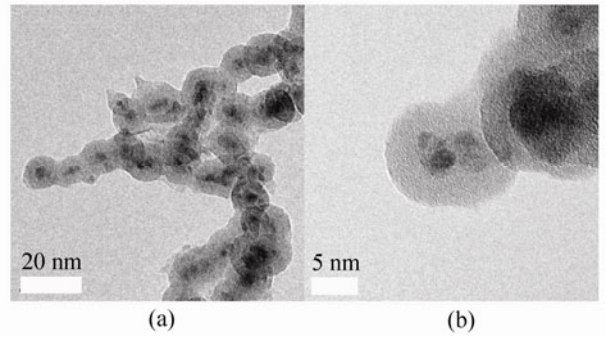

Figure 3 TEM images of Au/Co/Fe core–shell NPs with (a) low and (b) high magnification

shell layers. High resolution TEM images (Fig. 4 and Fig. S-1 in the Electronic Supplementary Material (ESM)) indicate that the sample consists of a crystalline Au core and amorphous Co and Fe outer layers. An HAADF-STEM image is shown in Fig. 5(a) and the corresponding EDS spectra are shown in Fig. 5(b). The EDS analysis reveals the Au:Co:Fe atomic ratio to be 6:6:88, which agrees well with the atomic ratio in the precursors. Only the EDS spectrum at the core part of the NPs (point 1) shows Au peaks, confirming that Au atoms exist only in the center of the NPs. Comparing the EDS spectrum at point 2 with the spectrum at point 3, there is a clear difference in the Co/Fe peak area ratio. The HAADF-STEM image and corresponding elemental maps obtained by EELS

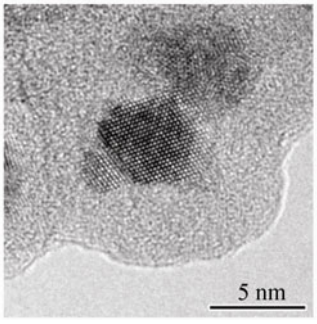

Figure 4 High resolution TEM image of the Au core of the Au/Co/Fe core–shell NPs

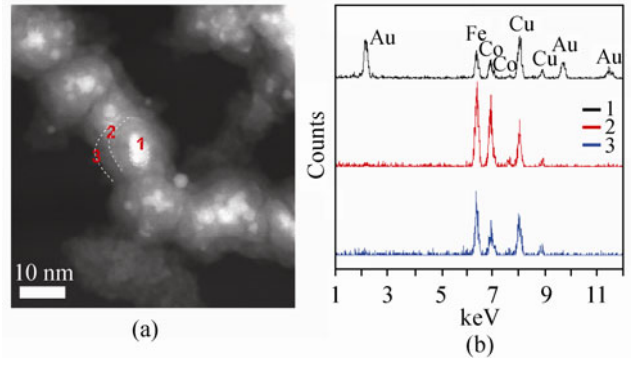

Figure 5 (a) HAADF-STEM of Au/Co/Fe triple-layered core–shell NPs. The broken line clearly shows the triple-layered structure. (b) The corresponding EDS spectra at the points indicated in (a)

measurements on the Au/Co/Fe triple-layered core–shell NPs also provide clear evidence that the core of the NPs is Au, whilst the inter-layer is Co-rich and the outer shell is Fe-rich (Fig. 6).

Powder XRD patterns of Au/Co/Fe NPs before and after heat treatment at 873 K for 5 h in a He atmosphere are shown in Fig. 7. After heat treatment, the amorphous Co and Fe outer layers became crystalline metallic Co and Fe (Fig. 7(b)). The weak XRD peaks characteristic of Fe_2O_3 might be due to the exposure of the samples to air during the treatment or/and measurements. The TEM and HAADF-STEM results revealed that the most of Au/Co/Fe NPs still retain the triple-layered core–shell structure after heat treatment (Figs. S-2 and S-3 in the ESM).

The catalytic properties of Au/Co/Fe core–shell NPs and those of the monometallic Au, Co, Fe and bimetallic Co/Fe, Au/Fe, Au/Co counterparts were compared using the hydrolytic dehydrogenation of AB as a probe reaction [22–36]. Figure S-4 (in the ESM) shows the mass analysis of the gases generated from the

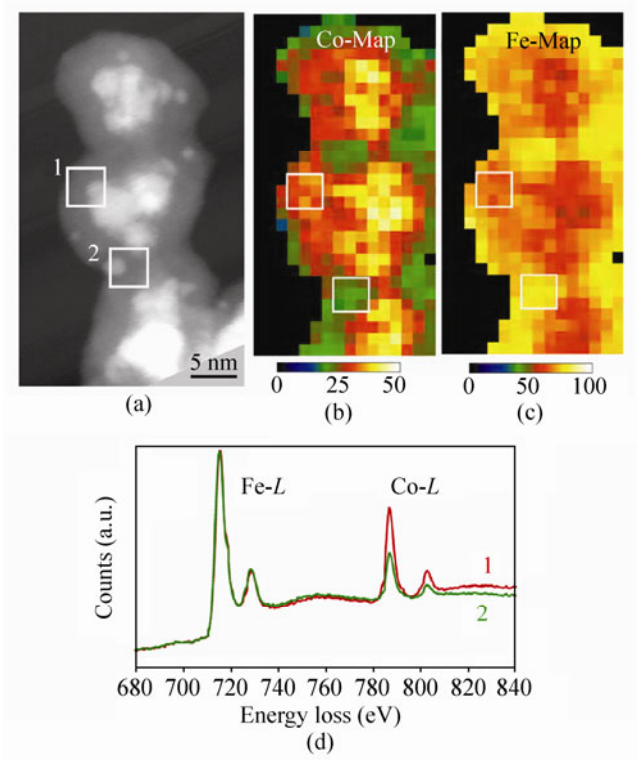

Figure 6 (a) HAADF-STEM image of Au/Co/Fe triple-layered core–shell NPs and corresponding elemental maps by EELS for (b) Co and (c) Fe, and (d) the EELS spectra at the areas indicated in (a). The bright parts in (a) show Au cores. The yellow parts in (b) indicate that the inter-layer is Co-rich. The yellow parts in (c) indicate that the outer shell is Fe-rich

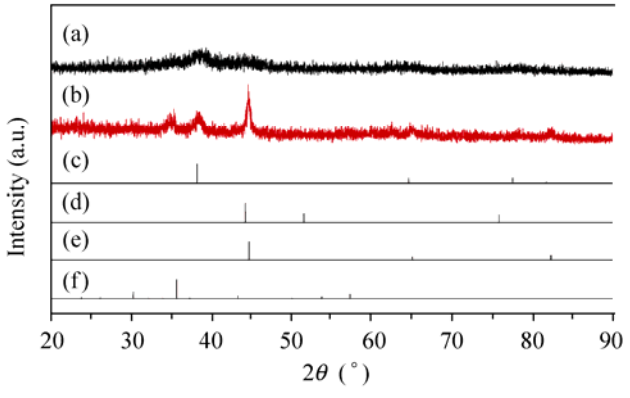

Figure 7 XRD patterns of Au/Co/Fe triple-layered core–shell NPs (a) before and (b) after heat treatment at 873 K for 5 h in a He atmosphere. The reference XRD patterns of (c) Au (powder diffraction file (PDF) 65-2870), (d) Co (PDF 15-0806), (e) Fe (PDF 06-0696), and (f) Fe_2O_3 (PDF 39-1346)

hydrolysis of AB (0.17 mol/L, 10.0 mL) catalyzed by Au/Co/Fe triple-layered core–shell NPs (Au = 0.012 mmol, Co = 0.012 mmol, and Fe = 0.176 mmol)

under an argon atmosphere at 298 K. It is obvious that the released gas was pure H_2. Gas phase ammonia (NH_3) and related species were not detected in the mass spectrum. The catalytic activities of monometallic Au, Co, and Fe catalysts are shown in Fig. 8. Only 70% of the maximum amount of hydrogen was released after 300 min with Au NP catalysts (Fig. 8(c)), and almost no H_2 release was observed with the Co catalyst and only 25% of the maximum amount of H_2 was released with the Fe catalyst in 200 min (Figs. 8(a) and 8(b)). These results indicate that the monometallic Co^{2+} and Fe^{3+} cations are not readily reduced by AB to Co and Fe to form active catalysts for AB hydrolytic dehydrogenation.

The catalytic activities of bimetallic Co/Fe, Au/Fe, Au/Co and trimetallic Au/Co/Fe NPs are displayed in Fig. 9. Both Co/Fe and Au/Fe catalysts (Figs. 9(a) and 9(b)) show catalytic activities similar to that of the monometallic Fe catalyst. The bimetallic Au/Co catalyst shows much better activity (Fig. 9(c)), indicating the formation of highly active Au@Co core–shell NPs as reported previously by us [16]: Au^{3+} was readily reduced by AB to yield Au NPs which catalyze the decomposition of AB to generate H_2 and active –H species, which further induce the reduction of Co^{2+} to Co seeds to give Au/Co core–shell NPs, which act as an active catalyst for the hydrolysis of AB [16]. In contrast, bimetallic Au/Fe and Co/Fe NPs show low catalytic activities, similar to that of the monometallic

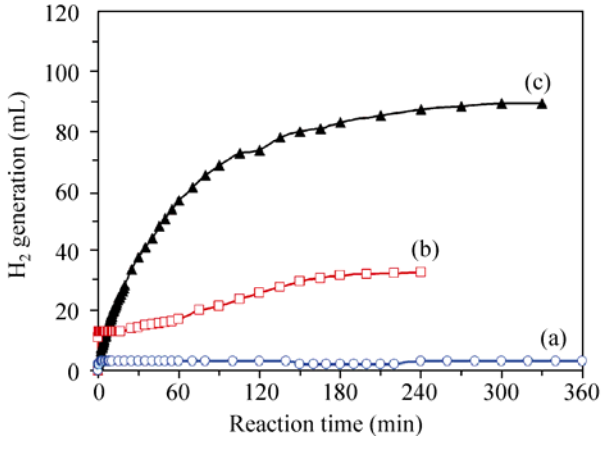

Figure 8 Hydrogen generation from aqueous AB solution (0.17 mol/L, 10.0 mL) catalyzed by (a) Co (0.012 mmol), (b) Fe (0.176 mmol), and (c) Au (0.012 mmol) monometallic NPs at room temperature

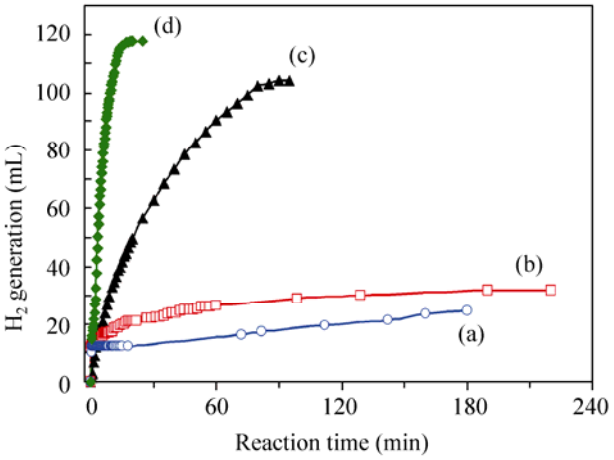

Figure 9 Hydrogen generation from aqueous AB solution (0.17 mol/L, 10.0 mL) catalyzed by (a) Co/Fe (Co = 0.012 mmol, Fe = 0.176 mmol), (b) Au/Fe (Au = 0.012 mmol, Fe = 0.176 mmol), (c) Au/Co (Au = 0.012 mmol, Co = 0.012 mmol) bimetallic NPs, and (d) Au/Co/Fe (Au = 0.012 mmol, Co = 0.012 mmol, and Fe = 0.176 mmol) trimetallic core–shell NPs at room temperature

Fe catalyst, indicating that the presence of single-component Au or Co is not sufficient to facilitate the reduction of Fe^{2+}.

In contrast to the observation that the presence of Au alone is not effective in facilitating the reduction of Fe^{2+} and the formation of an active Fe NP catalyst, the co-existence of small amounts of both Au and Co enhanced the reduction of Fe^{2+} and formed a highly active catalyst. As shown in Fig. 9(d), the Au/Co/Fe NPs exhibited the highest activity of all of the catalysts. In the presence of Au^{3+}, Co^{2+}, and Fe^{3+} cations, based on their reduction potentials AB can readily reduce Au^{3+} to Au and Fe^{3+} to Fe^{2+}. The resulting Au seeds catalyze the decomposition of AB to form hydrogen atoms and molecules which reduce Co^{2+} to Co to form the Co-rich layer around the Au core giving the Au/Co bimetallic core–shell NPs. Hydrogen atoms and molecules were rapidly produced due to the high catalytic activity of Au@Co NPs, which further enables the reduction of Fe^{2+} to Fe and the formation of the Fe-rich outer shell.

The theoretical molar ratio of hydrolytically generated hydrogen to AB is 3.0, corresponding to 127 mL H_2 evolution under our reaction conditions. The observed results indicate that the hydrolytic dehydrogenation was complete in the presence of

Au/Co/Fe trimetallic core–shell NPs (Fig. 9(d)), while in the presence of monometallic Au, Co, and Fe NPs and bimetallic Au/Co, Au/Fe, and Co/Fe NPs, the dehydrogenation was not complete. When a further equivalent amount of AB was added to the solution after the reaction in the presence of Au/Co bimetallic NPs, a further H_2 release of 98 mL was observed, however, as shown in Fig. S-5 (in the ESM). This volume is almost the same as that in the first run, indicating that the Au/Co bimetallic NPs retain their catalytic activity during the reaction. Furthermore, when highly active PtO_2 [27] was added to the solution after reaction no hydrogen release was observed (Fig. S-6(b) in the ESM), confirming that no unreacted AB was present. These two observations suggest that the incomplete dehydrogenation observed in the presence of the monometallic and bimetallic catalysts may possibly be a result of side-reactions, such as the dehydrogenation of AB (Eqs. (2) and (3)) [37–39]; these are known to occur in addition to the hydrolysis of AB (as shown by ^{11}B nuclear magnetic resonance (NMR) spectroscopy of the reaction solution in our previous report [12]).

$$NH_3BH_3 \longrightarrow H_2NBH_2 + H_2 \quad (2)$$

$$H_2NBH_2 \longrightarrow HNBH + H_2 \quad (3)$$

Smaller amounts of hydrogen (1 or 2 equiv.) are generated via these reactions than via hydrolysis of AB (3 equiv. of hydrogen). It has been observed with many catalysts, for example, palladium black [27], platinum- and nickel-based alloys [40], and gold-, nickel-, and copper-based catalysts [12, 41, 42], that less than a stoichiometric amount of hydrogen is generated, arising from the incomplete hydrolysis of AB.

High stability and easy recyclability are key requirements for practical catalysts. Magnetic NPs have the advantage of being easily separated by a magnet. During the reaction, the black particles were suspended in the aqueous solution (Fig. 10(a)), while after reaction the magnetic particles can be effectively congregated and separated by a magnet (Fig. 10(b)). The efficient magnetic separation is very useful for recycling of the catalyst, especially in solution systems.

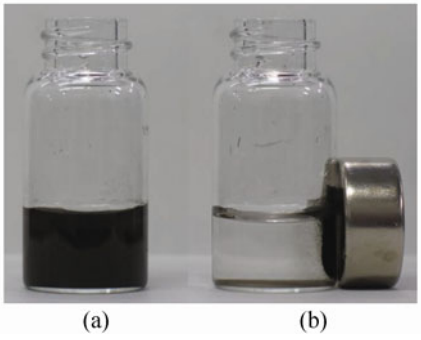

Figure 10 Photographs of the Au/Co/Fe core–shell NPs (a) before and (b) after magnetic separation

After the hydrogen generation reaction was complete, durability tests of the Au/Co/Fe NPs were conducted using magnetic decantation. Figure 11 shows the profiles of hydrogen generation from aqueous AB solution (0.17 mol/L, 10.0 mL) vs. reaction time catalyzed by *in situ* synthesized Au/Co/Fe NPs at room temperature over several runs with the addition of additional equivalent amounts of AB. Even after the 5th run, the Au/Co/Fe NPs maintained their initial catalytic activity. The structures and compositions of the reused catalyst were essentially the same as those of the initial material as confirmed by TEM, HAADF-STEM, and EDS measurements (Figs. S-7–S-9 in the ESM).

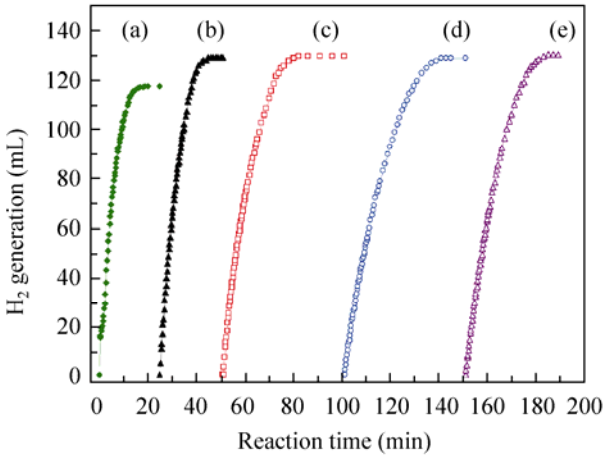

Figure 11 Hydrogen generation from aqueous AB solution (0.17 mol/L, 10.0 mL) catalyzed by Au/Co/Fe (Au = 0.012 mmol, Co = 0.012 mmol, and Fe = 0.176 mmol) trimetallic core–shell NPs at room temperature in the (a) 1st, (b) 2nd, (c) 3rd, (d) 4th, and (e) 5th runs carried out by addition of equivalent amounts of AB

4. Conclusions

We have developed the first one-step seeding-growth method for the synthesis of magnetic triple-layered core–shell Au/Co/Fe NPs at room temperature under ambient atmosphere. The resulting Au/Co/Fe NPs exhibit much higher catalytic activity for the hydrolytic dehydrogenation of ammonia borane than the corresponding mono- and bi-metallic NPs. This simple technique can be extended to other multi-metallic systems, which should be useful as optical, magnetic, and electrical materials as well as in heterogeneous catalysis.

Acknowledgements

We thank National Institute of Advanced Industrial Science and Technology (AIST), Kobe University and Japan Science and Technology Agency (JST) for financial support.

Electronic Supplementary Material: Supplementary material (characterization of Au/Co/Fe NPs by TEM, high resolution transmission electron microscopy (HRTEM), HAADF-STEM, and EDS, mass spectrum of released gases, catalytic AB hydrolysis experiments with Au/Co NPs) is available in the online version of this article at http://dx.doi.org/10.1007/s12274-011-0174-1.

References

[1] Toshima, N.; Harada, M.; Yonezawa, T.; Kushihashi, K.; Asakura, K. Structural analysis of polymer-protected Pd/Pt bimetallic clusters as dispersed catalysts by using extended X-ray absorption fine structure spectroscopy. *J. Phys. Chem.* **1991**, *95*, 7448–7453.

[2] Sun, Y. G.; Xia, Y. N. Shape-controlled synthesis of gold and silver nanoparticles. *Science* **2002**, *298*, 2176–2179.

[3] Toshima, N.; Kanemaru, M.; Shiraishi, Y.; Koga, Y. Spontaneous formation of core/shell bimetallic nanoparticles: A calorimetric study. *J. Phys. Chem. B* **2005**, *109*, 16326–16331.

[4] Wilson, O. M.; Scott, R. W. J.; Garcia-Martinez, J. C.; Crooks, R. M. Synthesis, characterization, and structure-selective extraction of 1–3-nm diameter AuAg dendrimer-encapsulated bimetallic nanoparticles. *J. Am. Chem. Soc.* **2005**, *127*, 1015–1024.

[5] Tao, F.; Grass, M. E.; Zhang, Y. W.; Butcher, D. R.; Renzas, J. R.; Liu, Z.; Chung, J. Y.; Mun, B. S.; Salmeron, M.; Somorjai, G. A. Reaction-driven restructuring of Rh–Pd and Pt–Pd core–shell nanoparticles. *Science* **2008**, *322*, 932–934.

[6] Alayoglu, S.; Nilekar, A. U.; Mavrikakis, M.; Eichhorn, B. Ru–Pt core–shell nanoparticles for preferential oxidation of carbon monoxide in hydrogen. *Nat. Mater.* **2008**, *7*, 333–338.

[7] Yang, J.; Sargent, E. H.; Kelley, S. O.; Ying, J. Y. A general phase-transfer protocol for metal ions and its application in nanocrystal synthesis. *Nat. Mater.* **2009**, *8*, 683–689.

[8] Lee, Y. W.; Kim, M.; Kim, Z. H.; Han, S. W. One-step synthesis of Au@Pd core–shell nanooctahedron. *J. Am. Chem. Soc.* **2009**, *131*, 17036–17037.

[9] Kobayashi, H.; Yamauchi, M.; Kitagawa, H.; Kubota, Y.; Kato, K.; Takata, M. Atomic-level Pd–Pt alloying and largely enhanced hydrogen-storage capacity in bimetallic nanoparticles reconstructed from core/shell structure by a process of hydrogen absorption/desorption. *J. Am. Chem. Soc.* **2010**, *132*, 5576–5577.

[10] Ferrando, R.; Jellinek, J.; Johnston, R. L. Nanoalloys: From theory to applications of alloy clusters and nanoparticles. *Chem. Rev.* **2008**, *108*, 845–910.

[11] Zhang, Z. Y.; Nenoff, T. M.; Leung, K.; Ferreira, S. R.; Huang, J. Y.; Berry, D. T.; Provencio, P. P.; Stumpft, R. Room-temperature synthesis of Ag–Ni and Pd–Ni alloy nanoparticles. *J. Phys. Chem. C* **2010**, *114*, 14309–14318.

[12] Jiang, H. L.; Umegaki, T.; Akita, T.; Zhang, X. B.; Haruta, M.; Xu, Q. Bimetallic Au–Ni nanoparticles embedded in SiO_2 nanospheres: Synergetic catalysis in hydrolytic dehydrogenation of ammonia borane. *Chem. Eur. J.* **2010**, *16*, 3132–3137.

[13] Wang, D. S.; Li, Y. D. One-pot protocol for Au-based hybrid magnetic nanostructures via a noble-metal-induced reduction process. *J. Am. Chem. Soc.* **2010**, *132*, 6280–6281.

[14] Jiang, H. L.; Akita, T.; Ishida, T.; Haruta, M.; Xu, Q. Synergistic catalysis of Au@Ag core–shell nanoparticles stabilized on metal-organic framework. *J. Am. Chem. Soc.* **2011**, *133*, 1304–1306.

[15] Yan, J. M.; Zhang, X. B.; Han, S.; Shioyama, H.; Xu, Q. Magnetically recyclable Fe–Ni alloy catalyzed dehydrogenation of ammonia borane in aqueous solution under ambient atmosphere. *J. Power Sources* **2009**, *194*, 478–481.

[16] Yan, J. M.; Zhang, X. B.; Akita, T.; Haruta, M.; Xu, Q. One-step seeding growth of magnetically recyclable Au@Co core–shell nanoparticles: Highly efficient catalyst for hydrolytic dehydrogenation of ammonia borane. *J. Am. Chem. Soc.* **2010**, *132*, 5326–5327.

[17] Mazumder, V.; Chi, M. F.; More, K. L.; Sun, S. H. Core/shell Pd/FePt nanoparticles as an active and durable catalyst for

the oxygen reduction reaction. *J. Am. Chem. Soc.* **2010**, *132*, 7848–7849.

[18] Toshima, N.; Ito, R.; Matsushita, T.; Shiraishi, Y. Trimetallic nanoparticles having a Au-core structure. *Catal. Today* **2007**, *122*, 239–244.

[19] Mazumder, V.; Chi, M. F.; More, K. L.; Sun, S. H. Synthesis and characterization of multimetallic Pd/Au and Pd/Au/FePt core/shell nanoparticles. *Angew. Chem. Int. Ed.* **2010**, *49*, 9368–9372.

[20] Wang, L.; Yamauchi, Y. Autoprogrammed synthesis of triple-layered Au@Pd@Pt core–shell nanoparticles consisting of a Au@Pd bimetallic core and nanoporous Pt Shell. *J. Am. Chem. Soc.* **2010**, *132*, 13636–13638.

[21] Kitchin, J. R.; Nørskov, J. K.; Barteau, M. A.; Chen, J. G. Role of strain and ligand effects in the modification of the electronic and chemical properties of bimetallic surfaces. *Phys. Rev. Lett.* **2004**, *93*, 156801.

[22] Hamilton, C. W.; Baker, R. T.; Staubitz, A.; Manners, I. B–N compounds for chemical hydrogen storage. *Chem. Soc. Rev.* **2009**, *38*, 279–293.

[23] Gutowska, A.; Li, L. Y.; Shin, Y. S.; Wang, C. M. M.; Li, X. H. S.; Linehan, J. C.; Smith, R. S.; Kay, B. D.; Schmid, B.; Shaw, W.; Gutowski, M.; Autrey, T. Nanoscaffold mediates hydrogen release and the reactivity of ammonia borane. *Angew. Chem. Int. Ed.* **2005**, *44*, 3578–3582.

[24] Bluhm, M. E.; Bradley, M. G.; Butterick, R.; Kusari, U.; Sneddon, L. G. Amineborane-based chemical hydrogen storage: Enhanced ammonia borane dehydrogenation in ionic liquids. *J. Am. Chem. Soc.* **2006**, *128*, 7748–7749.

[25] Diyabalanage, H. V. K.; Shrestha, R. P.; Semelsberger, T. A.; Scott, B. L.; Bowden, M. E.; Davis, B. L.; Burrell, A. K. Calcium amidotrihydroborate: A hydrogen storage material. *Angew. Chem. Int. Ed.* **2007**, *46*, 8995–8997.

[26] Xiong, Z. T.; Yong, C. K.; Wu, G. T.; Chen, P.; Shaw, W.; Karkamkar, A.; Autrey, T.; Jones, M. O.; Johnson, S. R.; Edwards, P. P.; David, W. I. F. High-capacity hydrogen storage in lithium and sodium amidoboranes. *Nat. Mater.* **2008**, *7*, 138–141.

[27] Chandra, M.; Xu, Q. A high-performance hydrogen generation system: Transition metal-catalyzed dissociation and hydrolysis of ammonia–borane. *J. Power Sources* **2006**, *156*, 190–194.

[28] Xu, Q.; Chandra, M. Catalytic activities of non-noble metals for hydrogen generation from aqueous ammonia–borane at room temperature. *J. Power Sources* **2006**, *163*, 364–370.

[29] Xu, Q.; Chandra, M. A portable hydrogen generation system: Catalytic hydrolysis of ammonia–borane. *J. Alloys. Compd.* **2007**, *446*, 729–732.

[30] Yan, J. M.; Zhang, X. B.; Han, S.; Shioyama, H.; Xu, Q. Iron-nanoparticle-catalyzed hydrolytic dehydrogenation of ammonia borane for chemical hydrogen storage. *Angew. Chem. Int. Ed.* **2008**, *47*, 2287–2289.

[31] Umegaki, T.; Yan, J. M.; Zhang, X. B.; Shioyama, H.; Kuriyama, N.; Xu, Q. Boron- and nitrogen-based chemical hydrogen storage materials. *Int. J. Hydrogen Energy* **2009**, *34*, 2303–2311.

[32] Jiang, H. L.; Singh, S. K.; Yan, J. M.; Zhang, X. B.; Xu, Q. Liquid-phase chemical hydrogen storage: Catalytic hydrogen generation under ambient conditions. *ChemSusChem* **2010**, *3*, 541–549.

[33] Metin, Ö.; Mazumder, V.; Özkar, S.; Sun, S. S. Monodisperse nickel nanoparticles and their catalysis in hydrolytic dehydrogenation of ammonia borane. *J. Am. Chem. Soc.* **2010**, *132*, 1468–1469.

[34] Çalışkan, S.; Zahmakıran, M.; Özkar, S. Zeolite confined rhodium(0) nanoclusters as highly active, reusable, and long-lived catalyst in the methanolysis of ammonia–borane. *Appl. Catal. B-Environ.* **2010**, *93*, 387–394.

[35] Demirci, U. B.; Miele, P. Hydrolysis of solid ammonia borane. *J. Power Sources* **2010**, *195*, 4030–4035.

[36] Jiang, H. L.; Xu, Q. Catalytic hydrolysis of ammonia borane for chemical hydrogen storage. *Catal. Today* **2011**, *170*, 56–63.

[37] Denney, M. C.; Pons, V.; Hebden, T. J.; Heinekey, D. M.; Goldberg, K. I. Efficient catalysis of ammonia borane dehydrogenation. *J. Am. Chem. Soc.* **2006**, *128*, 12048–12049.

[38] Keaton, R. J.; Blacquiere, J. M.; Baker, R. T. Base metal catalyzed dehydrogenation of ammonia–borane for chemical hydrogen storage. *J. Am. Chem. Soc.* **2007**, *129*, 1844–1845.

[39] Stephens, F. H.; Pons, V.; Baker, R. T. Ammonia-borane: The hydrogen source par excellence? *Dalton Trans.* **2007**, 2613–2626.

[40] Yao, C. F.; Zhuang, L.; Cao, Y. L.; Ai, X. P.; Yang, H. X. Hydrogen release from hydrolysis of borazane on Pt- and Ni-based alloy catalysts. *Int. J. Hydrogen Energy* **2008**, *33*, 2462–2467.

[41] Kalidindi, S. B.; Sanyal, U.; Jagirdar, B. R. Nanostructured Cu and Cu@Cu_2O core shell catalysts for hydrogen generation from ammonia-borane. *Phys. Chem. Chem. Phys.* **2008**, *10*, 5870–5874.

[42] Umegaki, T.; Yan, J. M.; Zhang, X. B.; Shioyama, H.; Kuriyama, N.; Xu, Q. Hollow Ni–SiO_2 nanosphere-catalyzed hydrolytic dehydrogenation of ammonia borane for chemical hydrogen storage. *J. Power Sources* **2009**, *191*, 209–216.